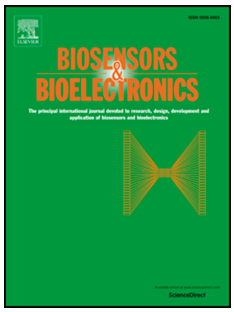

3D-printed reduced graphene oxide/polylactic acid electrodes: A new prototyped platform for sensing and biosensing applications

Vinicius A.O.P. da Silva, Wilson S. Fernandes-Junior, Diego P. Rocha, Jéssica S. Stefano, Rodrigo A.A. Munoz, Juliano A. Bonacin, Bruno C. Janegitz

PII: S0956-5663(20)30673-4

DOI: https://doi.org/10.1016/j.bios.2020.112684

Reference: BIOS 112684

To appear in: *Biosensors and Bioelectronics*

Received Date: 19 June 2020

Revised Date: 30 August 2020

Accepted Date: 2 October 2020

Please cite this article as: da Silva, V.A.O.P., Fernandes-Junior, W.S., Rocha, D.P., Stefano, Jé.S., Munoz, R.A.A., Bonacin, J.A., Janegitz, B.C., 3D-printed reduced graphene oxide/polylactic acid electrodes: A new prototyped platform for sensing and biosensing applications, *Biosensors and Bioelectronics* (2020), doi: https://doi.org/10.1016/j.bios.2020.112684.

Credit author statement

Vinicius A. O. P. da Silva – Formal analysis, Conceptualization, Validation, Investigation, Writing - Original Draft, Writing - Review & Editing

Wilson S. Fernandes-Junior - Formal analysis, Conceptualization, Validation, Investigation, Writing – Validation, Original Draft, Writing - Review & Editing

Diego P. Rocha - Conceptualization, Writing - Original Draft, Writing - Review & Editing

Jéssica S. Stefano - Conceptualization, Writing - Original Draft, Writing - Review & Editing

Rodrigo A. A. Munoz -Conceptualization, Writing - Original Draft, Writing - Review & Editing

Juliano A. Bonacin- Conceptualization Writing - Original Draft, Writing - Review & Editing

Bruno C. Janegitz – Conceptualization, Writing - Review & Editing, Supervision, Funding acquisition, Project administration

3D-printed reduced graphene oxide/polylactic acid electrodes: a new prototyped platform for sensing and biosensing applications

Vinicius A. O. P. da Silva[a], Wilson S. Fernandes-Junior [a], Diego P. Rocha[b], Jéssica S. Stefano[b], Rodrigo A. A. Munoz[b], Juliano A. Bonacin[c], Bruno C. Janegitz [a] *

[a] Department of Nature Sciences, Mathematics and Education, Federal University of São Carlos, 13600-970, Araras, São Paulo, Brazil

[b] Institute of Chemistry, Federal University of Uberlândia, 38400-902, Uberlândia, MG, Brazil.

[c] Institute of Chemistry, University of Campinas, P.O. Box 6154, 13083-970 Campinas, SP, Brazil

*Corresponding author: Prof. Bruno C. Janegitz

E-mail: brunocj@ufscar.br

Abstract

This work presents a novel procedure involving the sequential chemical treatment to generate reduced graphene oxide (rGO) within 3D-printed polylactic acid (PLA) electrodes and their potential applications for sensing and biosensing. A new configuration of a compact all-3D-printed electrochemical device containing the three electrodes is presented, in which the working electrode was treated to generate rGO within PLA (rGO-PLA) after treatment within $NaBH_4$. The rGO-PLA electrodes presented a notable current increase for the redox probe ferrocene-methanol in comparison with the same surface treated by dimethylformamide (DMF) immersion. Also, the electrochemical impedance spectroscopic data that presented the lowest resistance to electron transfer for the proposed electrode. The electrochemical experiments were in accordance with Raman spectra and surface roughness obtained by atomic force microscopy (AFM) images. As proofs-of-concept, the rGO-PLA electrode was applied for serotonin determination in synthetic urine using differential-pulse voltammetry with a limit of detection of 0.032 μmol L^{-1}. Also, the second application involved the fabrication of a tyrosinase biosensor capable of determining catechol in natural water samples with a limit of detection of 0.26 μmol L^{-1}. Based on both applications, the 3D-printed rGO-PLA showed to be an excellent platform for biosensing purposes.

Keywords: reduced graphene oxide; biosensor; phenol; 3D-electrodes

1. Introduction

Three-dimensional (3D) printing has generated a revolution in the fabrication of multifaceted objects applied in different areas, such as electronics, medicine, biotechnology, engineering, aerospace, and chemistry (Ngo et al., 2018). In the chemistry area, many efforts have been reported in the literature, and some of them are compiled in recent revisions, for instance demonstrating the potential applications of 3D-printing technologies to prototype milli- and microfluidic analytical devices (Au et al., 2016; Cocovi-Solberg et al., 2018; Nielsen et al., 2020), energy storage devices (Gulzar et al., 2019; Pang et al., 2020), and electrochemical sensors (Cardoso et al., 2020a; Hamzah et al., 2018; Katic et al., 2019; O'Neil, 2020). For example, Manzanares-Palenzuela and coauthors have proposed an elegant way to manufacture a biosensor by immobilization of enzyme alkaline phosphatase for electrochemical detection of 1-naphthol in aqueous media (Manzanares-Palenzuela et al., 2019).

Conductive polymers or conducting thermoplastic filaments play a key role in the development of electrochemical sensing and energy storage devices using 3D-printing technology (Cardoso et al., 2020a; Gulzar et al., 2019; Pang et al., 2020). Mostly employed conductive thermoplastic filaments for 3D-printing consist of composite materials typically composed of polylactic acid (PLA) or acrylonitrile butadiene styrene (ABS) with a conducting agent, such as graphene or carbon black (Cardoso et al., 2020a; Hamzah et al., 2018). Alternatively, lab-made conductive thermoplastic filaments (filaments manufactured in the laboratory, that is, not purchased commercially) have been proposed for 3D-printing with applications to electrochemical

sensors (Foster et al., 2020; Honeychurch et al., 2018; Diego Pessoa Rocha et al., 2020) and water splitting (Hughes et al., 2020).

The 3D-printed electrodes present in their composition large amounts of insulating polymeric material (Cardoso et al., 2020a). To remove the non-conductive thermoplastic materials, expose the conductive sites, and improve the electrochemical performance of the 3D-printed electrodes, a chemical surface treatment may be required. Various treatments have been reported in the literature, such as mechanical polishing (Cardoso et al., 2020b, 2019, 2018; Diego Pessoa Rocha et al., 2020), activation *via* an electrochemical protocol (dos Santos et al., 2019), chemical activation using different solvents (Gusmão et al., 2019), chemical and electrochemical sequentially employed activations (Browne et al., 2018). Also, it has been reported the treatments thermal and electrochemical sequentially employed activations (Novotný et al., 2019), *via* protein digestion (Manzanares-Palenzuela et al., 2019), *via* hydroxide ions (OH^-) produced by water electrolysis (Wirth et al., 2019), and concomitantly chemical/electrochemical activations (Richter et al., 2019; Diego P Rocha et al., 2020). A recent work compared most of these procedures for the surface treatment of such 3D-printed carbon electrodes and the authors stated that a treatment protocol using DMF solvent was more efficient to remove the insulating PLA to obtain high conductive sites improving the electrochemical performance of the proposed sensors (Kalinke et al. 2020).

Special attention has been given to 3D-printed carbon electrodes due to the high electron transfer of neurotransmitters on carbon surfaces facilitated by an adsorptive step (Yang et al., 2018). However, carbon electrodes may not be entirely selective for the detection of a single species in different biological media as other molecules also undergo electrochemical oxidation processes on the same surface. For example,

ascorbic acid, dopamine, serotonin, epinephrine, norepinephrine are present in brain slice (Yang et al., 2018); uric acid and nitrite in urine and saliva (Cardoso et al., 2020b); and dopamine in synthetic urine and human serum (Kalinke et al., 2020). For this reason, the development of electrochemical sensors/biosensors is essential to obtain highly selective sensors to be applied in such complex media. Some examples of 3D-printed electrochemical biosensors were recently presented in the literature (Adams et al., 2018; Cardoso et al., 2020b; Katseli et al., 2019; López Marzo et al., 2020). Three of these examples demonstrated the feasible immobilization of glucose oxidase on 3D-printed graphene/polylactic acid (PLA) (Adams et al., 2018; Cardoso et al., 2020b) and carbon-black/PLA (Katseli et al., 2019) electrodes for glucose biosensing in biological fluids. At the same time, the fourth one reported the immobilization of horseradish peroxidase on a gold-nanoparticles modified 3D-printed graphene/PLA (López Marzo et al., 2020). The incorporation of gold nanoparticles on the 3D-printed surface in the last example was justified to increase the sensitivity and detectability of the electrochemical biosensor. However, this strategy configures as an additional step in the development of the biosensor that increases the time and cost for preparation and includes the other source of error that may compromise reproducibility.

In this context, we present for the first time a new protocol for the synthesis and application of 3D-printed reduced graphene oxide/PLA electrodes (rGO-PLA). This approach consists of a novel platform with improved detectability to develop electrochemical biosensors as well as for the direct monitoring of biomolecules in complex media. Moreover, we propose a novel design of a complete electrochemical sensing platform composed of three electrodes (working, pseudo-reference, and counter electrodes) and the electrochemical cell via a single-step fabrication using fused deposition modeling (FDM). As proofs-of-concept, we demonstrate the electrochemical

biosensing of catechol (a contaminant that may be found in natural waters from industrial effluent discharges with a potential hazard for human health (Camargo et al., 2018)) in natural waters after immobilization of tyrosinase on the 3D-printed rGO-PLA surface and the direct enzymeless detection of serotonin (one of the most important neurotransmitters of the human body, in which abnormal levels can lead to various disorders and diseases (Sharma et al., 2018)) in the urine.

2. Experimental

2.1. Chemicals, solutions, and samples

Calcium chloride dihydrate (≥ 99 % m/m), potassium chloride (≥ 99 % m/m), creatinine (≥ 98.5 % m/m), ferrocene methanol (97 % m/m), serotonin (98 % m/m), dopamine hydrochloride (98 % m/m), uric acid (99 % m/m), (–)-epinephrine (95 % m/m), hydroquinone (99.5 % m/m), sodium nitrate (99 % m/m) anhydrous sodium sulfate (99 % m/m), urea (99 % m/m), dihexadecyl phosphate (99 % m/m), tyrosinase from mushroom with declared activity of 1000 units mg^{-1}, and pyrocatechol (99 % m/m) were purchased from Sigma-Aldrich (St. Louis, USA). Lead (II) nitrate (99.5 % m/m) was purchased from Merck (Darmstadt, Germany). Sodium chloride (99 % m/m), L-ascorbic acid (99 % m/m) mono and bibasic sodium phosphate anhydrous (≥ 98 % m/m and 99 % m/m, respectively) from Synth (Diadema, Brazil), ammonium chloride (99.5 % m/m) and dimethylformamide (99.8 % v/v) were obtained from Dinamica Química (Indaiatuba, Brazil). Sodium borohydride (99 % v/v), nitric acid (65 % v/v), and ethanol (99.5 % v/v) were obtained from Fluka (St. Louis, USA), Isofar (Duque de Caxias, Brazil), and Qhemis (Indaiatuba, Brazil), respectively. Colorless nail polish for

nail care was used for isolation of the sensor surface (Base Brilho Cuidados, Cora©, São Paulo, Brazil) (de Araujo Andreotti et al., 2019), being composed of butyl acetate, ethyl acetate, nitrocellulose, acetyl tributyl-citrate, toluene, isopropyl alcohol, tosylamide/formaldehyde resin, stearalkonium hectorite alcohol, hydrated silica, and mineral oil.

All standard and working solutions were prepared using at least 18.2 MΩ cm deionized water from a Heal Force® purification system. A solution containing 0.2 mol L^{-1} phosphate buffer was used as a background electrolyte for both direct voltammetric sensing serotonin (pH 7.0) and biosensing of catechol (pH 6.0). The working solutions were prepared daily by diluting the stock solutions in the supporting electrolyte just before the experiments. All studies were conducted without removing oxygen and at room temperature.

The serotonin sensor was applied towards serotonin sensing in synthetic urine samples. In this sense, synthetic urine was prepared according to the adaptation of a protocol proposed by Laube and collaborators (Laube et al., 2001). For this, a mixture of $CaCl_2.2H_2O$ (1.13 g L^{-1}), urea (25 g L^{-1}), NaH_2PO_4 (1.4 g L^{-1}), NaCl (2.92 g L^{-1}), Na_2SO_4 (2.25 g L^{-1}), KCl (1.6 g L^{-1}), NH_4Cl (1.0 g L^{-1}), and creatinine (1.1 g L^{-1}) was dissolved in 0.2 mol L^{-1} phosphate buffer solution (pH=6.0). The biosensor performance was evaluated through the catechol biosensing in artesian well water samples collected at Federal University of São Carlos – Araras *campus* (–22.315155, –47.380821), distribution water samples collected at Araras city (–22.35733, –47.3855874), and lake water samples collected at Ecological and Cultural Park "Gilberto Rüegger Ometto" (–22.3660008, –47.3572829) located at Araras city. For this, initially, the influence of the Tyr-DHP film in the presence of catechol was evaluated through cyclic voltammetry. Then, the square wave voltammetry (SWV) technique was used to obtain

a calibration curve for catechol under optimized conditions and further quantification of the fortified water samples.

2.2. Apparatus, electrochemical cell, and electrodes

All electrochemical measurements were acquired on both potentiostat/galvanostat PGSTAT204 Metrohm (Eco Chemie) guided by a software called NOVA (version 2.1.4), which was also used for data acquisition and treatment. Background-correction was used for voltammetric detection of serotonin and catechol for better viewing of the peaks, the treatment was performed using the "moving average" algorithm, with window size set to 2, available in the software NOVA (version 2.1.4).

A Sethi3D S3 3D printer (Campinas, Brazil), fed by both conductive (polylactic acid (PLA) doped with graphene acquired from Black Magic 3D (New York, USA)) and non-conductive (PLA from Sethi3D (Campinas, Brazil)) thermoplastic filaments, was used for the manufacture by fused deposition modeling (FDM) of the fully 3D-printed electrochemical system. A 30 mL lab-made electrochemical cell, with 46 mm diameter and 35 mm height, an inner diameter of 40 mm, and intern height of 32 mm was designed on Autodesk Inventor® Professional software and printed using the non-conductive PLA filament. The top part of the cell was printed in the form of a screw cap to fix the cover which also had this shape on the inner part. The cover of the electrochemical cell had 49 mm diameter, 8 mm height, and contained 5 holes of 8 mm diameter each for accomodating the arrangement of three electrodes (working, pseudo-reference, and counter electrodes). The three electrodes were designed using the same software used for the electrochemical cell and printed applying the conductive

graphene/PLA filament into the 3D printer to form three conductive hollow cylinders corresponding to the working, counter, and reference electrodes separately from the body of the cell through FDM manufacturing process. Those cylinders were removable and could be attached to the cover of the cell (made with non-conductive PLA), and the holes on each cylinder were designed to fit the potentiostat cables. Each electrode had 37.747 mm length with a 23 mm deep hollow for the connection with potentiostat cables. The inner diameter (diameter of the hollow) was 4.5 mm, while the external diameter was 7.5 mm. The counter electrode had the same shape as the others. However, on the top, an arc was designed for increasing the area for the occurrence of inverse redox reactions (to ensure that current does not pass through the pseudo-reference electrode during measurements), as shown in Figure S1 A and B (III). The arc was printed together with the body of this electrode and had 47.12 mm length, 5 mm height and its thickness was 1 mm. The electrode arrangement in the electrochemical cell is shown in Figure S1 A (software-generated image) and B (real image). Figure S1 C shows the assembled cell without connection to the potentiostat, and Figure S1 D a real image of the coupling between the fully 3D-printed electrochemical system and connectors of the equipment, being possible to observe that the electrodes are hollow (in the form of a cylinder) allowing the equipment connector to be directly connected to the electrodes as above-discussed. An insulating material (nail polish-based) was applied to the body of the cylindrical electrode, leaving uncovered only the lower rounded face of the electrodes for electron transfer. Hence, the geometric area of the rounded working electrode was 0.44 cm^2 in all measurements. All STL files were generated using the Simplify 3D software. For better comprehension of the whole process, a time-lapsed video showing the printing process of the cell and electrodes, including the assembling and connection to the potentiostat is available. The printing process enables the

obtention of approximately 2.3 sensors/h, for a cost of US$ 5.9, which could show availability to mass-produce the sensors.

2.3. Enhancement of the electrochemical performance of the graphene/polylactic acid (G-PLA) 3D-printed working electrode

After printing, the native G-PLA 3D-printed working, counter and reference electrodes were immersed in DMF for 15 minutes, washed with ethanol during 5 seconds to remove DMF residues, and then kept at room temperature in a Petri dish during ~~for~~ 24 hours for drying (Manzanares Palenzuela et al., 2018). Next, only the working electrode was immersed sequentially in two aqueous solutions: 1.0 mol L^{-1} nitric acid and 0.15 mol L^{-1} sodium borohydride (in each one for 15 minutes), respectively (Janegitz et al., 2014). Figure 1A displays the sequence of all steps in the process of obtaining the treated working electrode.

2.4. Fabrication of the biosensor upon the treated 3D-printed G-PLA electrodes

The treated G-PLA working electrode was used as a substrate for the biosensor manufacture. Thus, in a first step, for the preparation of the enzyme layer ~~bio~~film, the dihexadecyl phosphate (DHP) was dissolved in 0.2 mol L^{-1} phosphate buffer (pH 6.0) to achieve a final concentration of 1.0 mg mL^{-1}. Exactly 90 µL of this solution was mixed with the enzyme tyrosinase (10 µL/25 units) under constant stirring per 10 seconds. Next, a volume of 40 µL of the~~i~~s solution was placed, using a micropipette, upon the treated G-PLA surface. The biosensor was then kept inside a refrigerator for

drying for 48 hours before electrochemical measurements. The procedure is described in Figure 1B.

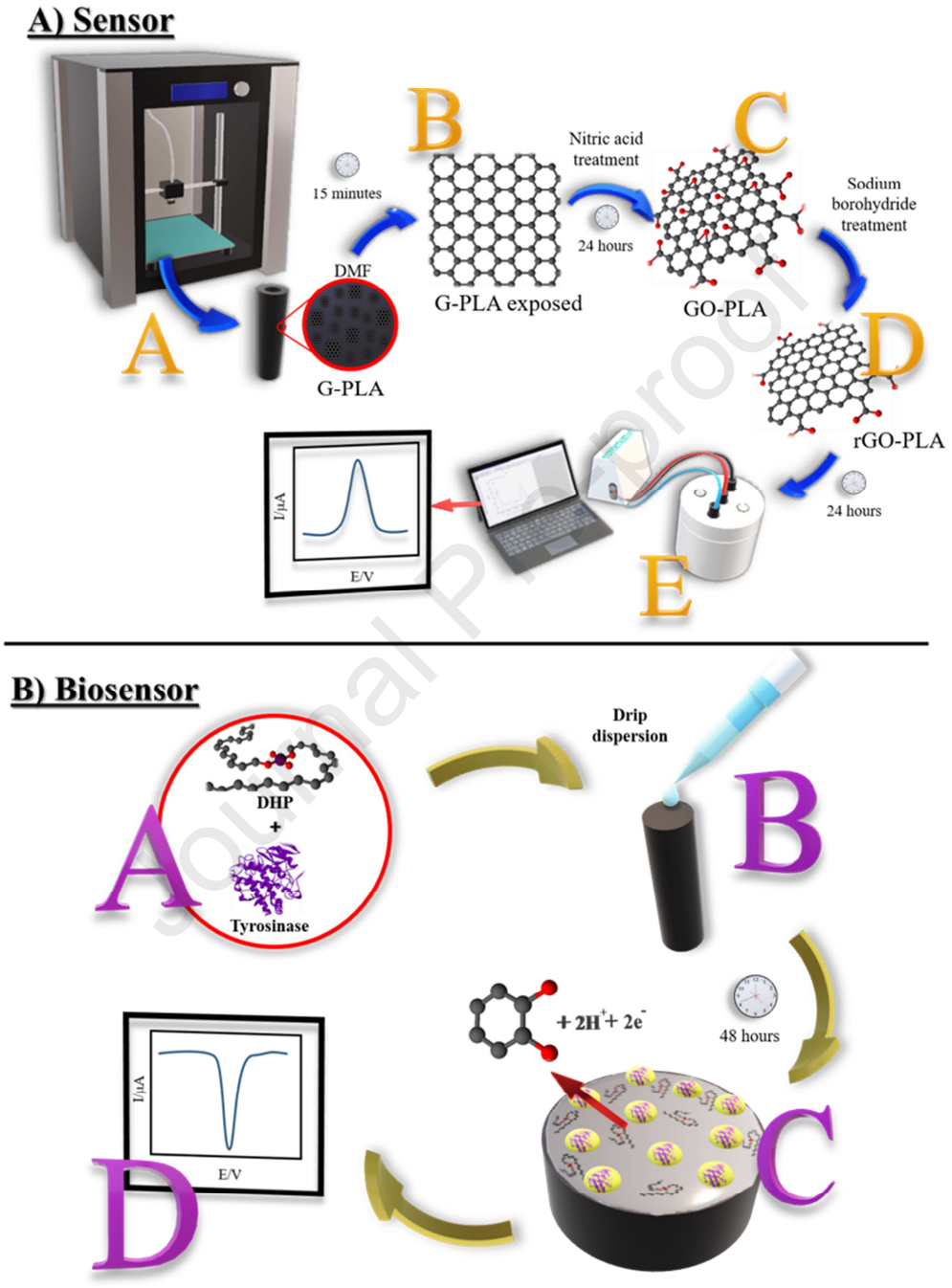

Figure 1. A) Scheme of the procedure for obtaining the G-PLA 3D-printed working, counter, and reference electrodes (A) and the sequence of chemical treatments performed on the working electrode (DMF treated in B; HNO_3 treated in C and sodium

borohydride treated in D), ~~(B-D).~~ and finally the assembled 3D-printed electrochemical cell connected to the apparatus for the acquisition of the analytical signal (E). **B)** Scheme of the steps involved in the production of the biosensor, including the mixture of DHP and tyrosinase (A), followed by the drop-casting of the modifiers on the working electrode surface (B) forming the film at the electrode surface (C) until obtention of the analytical signal (~~A-~~D).

2.5. Characterization of G-PLA electrode

The scanning electron microscopy (SEM) data were obtained using the XL-30 FEG microscope (Philips). Chemical mapping was obtained by energy-dispersive X-ray spectroscopy (EDS) coupled to a scanning electron microscope. Atomic force microscopy (AFM) measurements were obtained from a Shimadzu Scanning Probe Microscope (SPM-9600) using the tapping-mode to study the sample surface. The Raman spectra were acquired in a LabRAM HR Evolution spectrophotometer (HORIBA), using a 532 nm laser at 50 mW power over the 3500 – 800 cm^{-1} range. The characterization by X-ray diffractometry (XRD) was performed using a Miniflex 600 diffractometer (Rigaku), using a CuKα radiation source (λ = 0.15406 nm) 40 kV, from 4º to 90º angular recording range, with a step of 0.02º and 10º min^{-1} analysis time.

Electrochemical characterization was also performed *via* cyclic voltammetry and electrochemical impedance spectroscopy (EIS) measurements. The EIS measurements were performed in the presence of 1 mmol L^{-1} FcMeOH and 0.1 mol L^{-1} KCl solution, and the data was acquired using the FRA2 module coupled to the Autolab PGSTAT204 (Metrohm) controlled by the software NOVA 2.1. The frequency was used in the range

between 100 kHz and 100 mHz, and a perturbation amplitude of 10 mV was applied with 10 data points per frequency decade.

3. Results and discussion

3.1. Electrochemical performance of the reduced graphene oxide /polylactic acid (G-PLA) 3D-printed working electrode

After the electrodes were printed, they were attached to the electrochemical apparatus, and the performance of the system was evaluated via cyclic voltammetry using as redox probe 1.0 mmol L^{-1} ferrocene methanol (FcMeOH). Figure 2 presents the obtained results. As can be seen, the untreated G-PLA (green line) provided resistive behavior (poor electrochemical response), resulting in noisy response, making its use unfeasible for analytical purposes. In this sense, aiming to improve the electrochemical performance of the G-PLA, it was performed the method proposed by Manzanares *et al*. (immersion in DMF for 15 min) (Manzanares Palenzuela et al., 2018). It is possible to observe (purple line) the enhancement in the electrochemical behavior of the redox probe (about 18.0 % higher than in the native electrode considering the anodic peak current). However, after performing the treatment proposed by Manzanares *et al*. (Manzanares Palenzuela et al., 2018) followed by the chemical treatment using nitric acid followed by sodium borohydride as proposed in the literature to synthesize reduced graphene oxide (rGO) (Janegitz et al., 2014) (red line), the acquired results were much better among all regarding the anodic and cathodic peak currents and reversibility

(peak-to-peak separation (ΔEp)). The comparison between I_p and ΔE_p is shown in Table S1. Thereby, DMF immersion treatment followed by immersion in nitric acid and then sodium borohydride was carried out before all electrochemical measurements. Immersion time studies of the sensor in DMF were carried out at 5, 10, and 15 minutes, once after 15 minutes of immersion, the electrodes have broken. Therefore, 15 minutes was selected, which presented a better electrochemical response. The electrochemical results corresponding to each immersion time were recorded using cyclic voltammetry technique in presence of 2.0 mmol L^{-1} $[Fe(CN)_6]^{3-/4-}$ and 0.1 mol L^{-1} KCl solution at a scan rate of 50 mV s^{-1} and the results are shown in Figure S2.

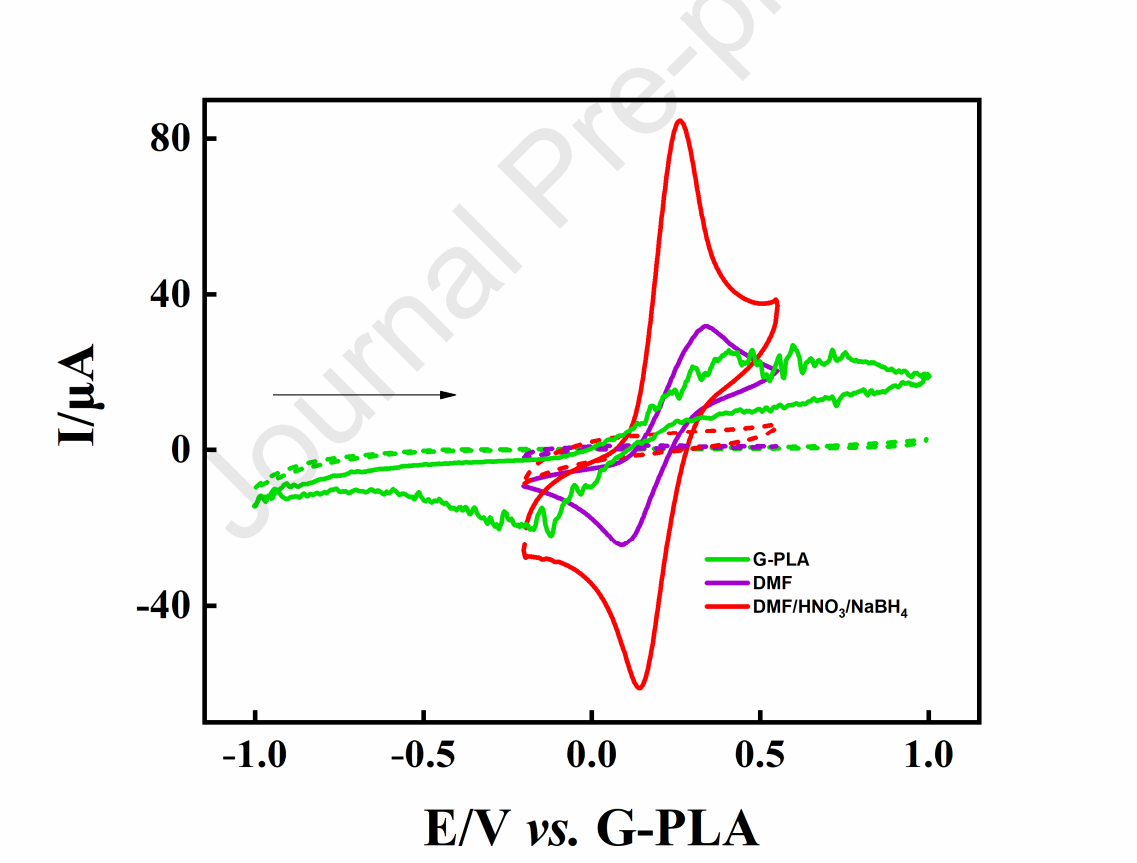

Figure 2. Cyclic voltammogram recordings obtained with native G-PLA (green line), G-PLA treated with DMF (purple line) and G-PLA treated with $DMF/HNO_3/NaBH_4$ (red line) in the presence of an equimolar solution of FcMeOH (1.0 mmol L^{-1}) containing 0.1 mol L^{-1} KCl. Dashed lines correspond to the respective blanks

(voltammograms recorded only in the background electrolyte (0.1 mol L^{-1} KCl), in the absence of FcMeOH (1.0 mmol L^{-1})). Scan rate: 50 mV s^{-1}. The potential range of the cyclic voltammogram performed on the native G-PLA was expanded (between -1.0 and 1.0 V), for the oxidation and reduction process occur completely. The voltammetric recordings were performed versus a pseudo-reference electrode (G-PLA).

To explain the results achieved in Figure 2, the surfaces of the native G-PLA, G-PLA/DMF, and rGO-PLA were carefully studied using characterization techniques. Figure 3 shows the images obtained for SEM analysis considering two magnification factors: 20000x (A-D) and 5000x (A'-D'). It is possible to observe in A (native G-PLA) a surface completely covered by the insulating thermoplastic polymer PLA, not being possible to observe the conductive sites composed by graphene. Similar results for the native G-PLA were observed in studies published in the literature (Browne et al., 2018; López Marzo et al., 2020; Manzanares-Palenzuela et al., 2019; Manzanares Palenzuela et al., 2018; Novotný et al., 2019). This result can be directly related to that obtained by cyclic voltammetry analysis (Figure 2 (green line)), in which poor electrochemical performance was obtained due to practically no availability of graphene at the surface of untreated G-PLA. In B, after immersion in DMF, it is possible to see that the solvent was able to remove a large amount of PLA and expose the graphene structures (Browne et al., 2018; López Marzo et al., 2020; Manzanares Palenzuela et al., 2018; Novotný et al., 2019), this was better observed in B', where a notable difference from native G-PLA is presented (comparison to A') improving the electrochemical performance of the G-PLA treated with DMF (as can be seen in Figure 2 (purple line)). Nevertheless, after the nitric acid treatment in the next step, the morphological changes were not so significant, and no differences were observed from B to C even when a SEM image with different

magnification factor was obtained (B' to C'). The same occurred after treatment with $NaBH_4$ (D and D'), where no significant structural differences were observed. However, an electrochemical improvement of the signal was observed after $NaBH_4$ treatment, as can be seen in the cyclic voltammograms (Figure 2 red line). Although the structure was not changing, a great increase in electrochemical response was observed, thus, this improvement of current response may not be related to changes in the structural morphology of the treated surface.

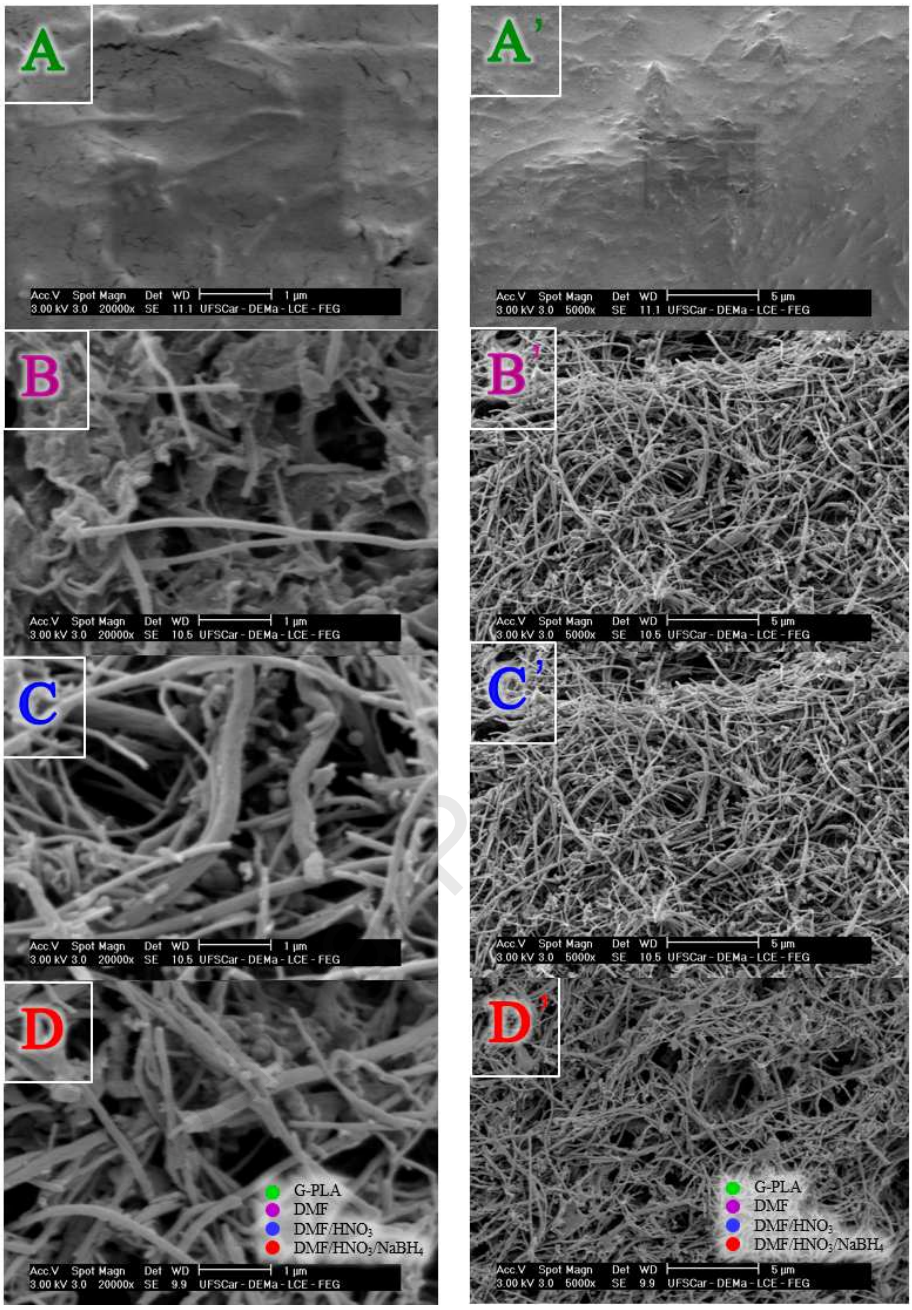

Figure 3. SEM images of electrode surfaces with different approximation factors: 20000x magnification (A-D) and 5000x magnification (A'-D').

The Raman spectra for each treatment step on the G-PLA surface are shown in Figure 4 A. These analyses were conducted to evaluate the changes provided by the chemical processes of the 3D-printed G-PLA treated with $DMF/HNO_3/NaBH_4$ and to confirm the formation of rGO. The characteristic bands D, G, and 2D present on

graphitic materials were observed, as reported by Browne and co-authors (Browne et al., 2018) whose employed Raman spectroscopy to characterize a 3D-printed graphene-based electrode without treatment. The D band at 1350 cm^{-1} was attributed to the out-of-plane vibrations in the graphitic lattice, therefore related to the presence of disordered carbons or defects in the graphene structure, while the G band at 1580 cm^{-1} was attributed to the in-plane stretching in sp^2 bonded carbon from those materials (Browne et al., 2018). The intensity ratio of D and G bands (I_D/I_G) indicated the density of defects and graphitization degree of the material, with higher values of I_D/I_G indicating the higher density of defects and small graphitization degree (Chen et al., 2020; Rocha et al., 2018a, 2018b). The presence of a 2D band at 2700 cm^{-1} was related to the presence of a multilayer of graphene, and the higher intensity of the 2D band indicated a larger number of graphene layers in the material (Rocha et al., 2018a, 2018b). It is possible to observe a variation in intensity on the D band throughout the treatment process. When the surface was treated only with DMF (Fig. 4A (purple line)) an intensity of 1050 a.u. was observed. The addition of a treatment step with HNO_3 (Fig. 4A (blue line)) provided an increase in the intensity to 1300 a.u., which indicated a higher quantity of defects and a less organized structure, also demonstrated by the increase in the I_D/I_G ratio (from 0.59 to 0.66). When $NaBH_4$ was employed for the reduction of the graphene oxide in the last step to generate rGO within the PLA matrix (Fig. 4A (red line)), the I_D/I_G ratio suffers a decrease from 0.66 to 0.56, and the intensity of the D band is again reduced (from 1300 to 870 a.u.). After each step of treatment, the intensity of the D band was changing considerably, alterations in the intensity up to 33% was observed, reaching a low intensity D band afterwards, which could indicate an organized structure. Therefore, the organization of the material is again established, and fewer defects in its structure is observed.

The reestablishment observed by Raman data can also be noted through the surface roughness of the material obtained from AFM images (Fig. 4B-E). After the treatment with DMF and DMF/HNO_3, the presence of defects provided a rougher surface compared to native-GPLA, from 0.194 ~~(Fig 5a)~~ (Fig. 4B) to 0.383 µm (Fig. 4C and 4D), indicating that those treatments decreased the organization of the material. In agreement with Raman data, the last step for reduction of the graphene oxide with $NaBH_4$ presented a reorganization of the structure, confirmed by the decrease in the roughness of the surface after the treatment to 0.285 µm (Fig. 4E), which resulted in a smoother surface at the end of the treatment process, as observed by dos Santos and colleagues (dos Santos et al., 2019). Thus, based on previously discussed data, there was strong evidence of the formation of rGO within PLA after the proposed treatments, and this process has led to even better results than those obtained employing the well-established procedure in the literature using only the DMF solvent (Figure 2 (red line)).

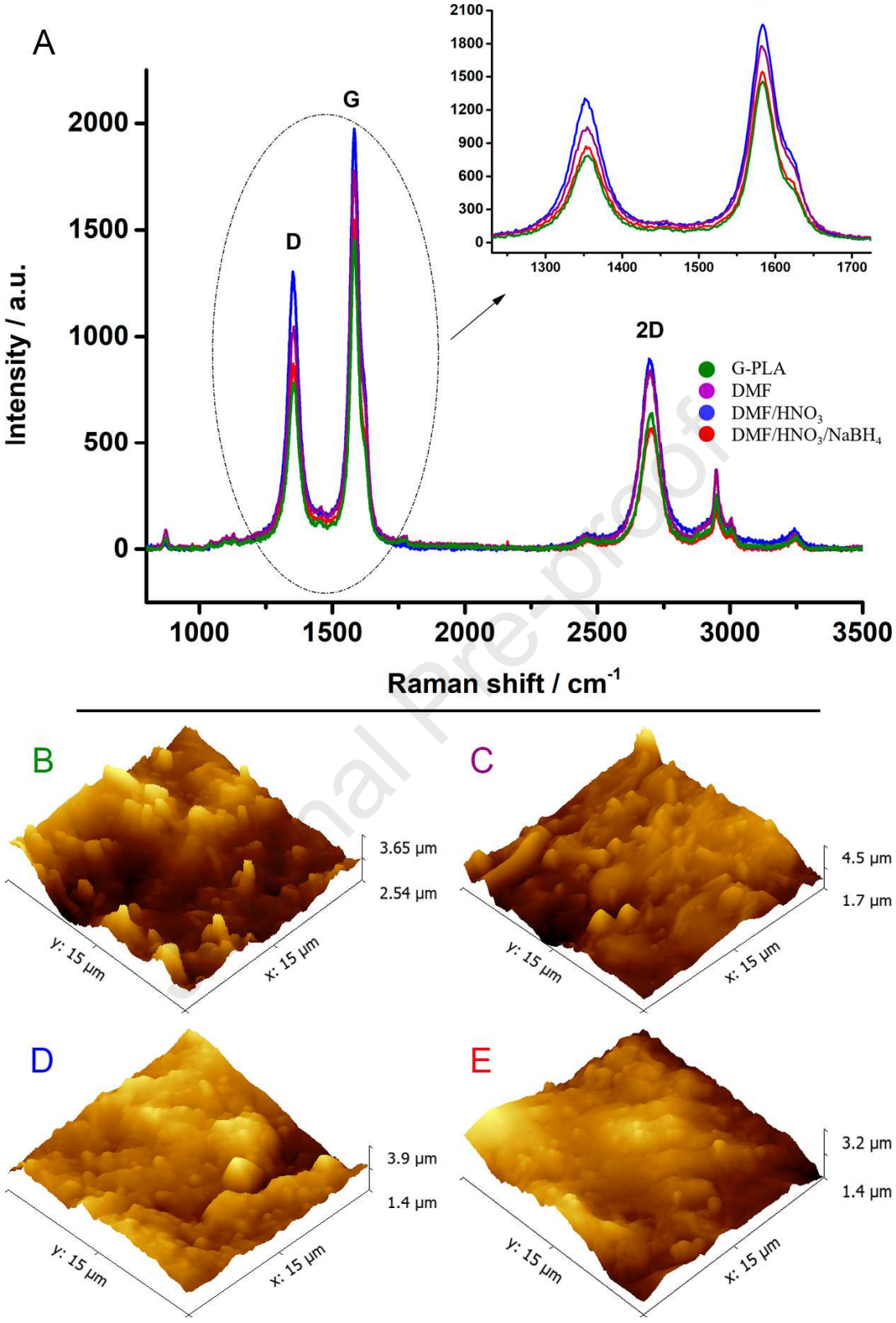

Figure 4. (A) Raman spectra for native (—); G-PLA treated with DMF (—); G-PLA/DMF/HNO_3 (—); G-PLA/DMF/HNO_3/$NaBH_4$ (—). (B-E) AFM images for native

G-PLA (B); G-PLA treated with DMF (C); G-PLA/DMF/HNO_3 (D); G-PLA/DMF/HNO_3/$NaBH_4$ (E) (rGO-PLA).

EIS technique was used to obtain a detailed understanding of the electrical characteristics of the electrode/solution interface of the native G-PLA electrodes. Also, measurements were carried out after the chemical treatment on the 3D-printed working electrode surface since the treatment process changes the capacitance of the double layer and the resistance to electron transfer of the electrode (Rocha et al., 2018a, 2018b). The results are displayed in Figure S3. It is noted that the native G-PLA (red circle) provided a higher diameter of the Nyquist semicircle with a charge transfer resistance (Rct) value of 1880 Ω. This resistive behavior of native G-PLA has also been reported in works previously published in the literature (Browne et al., 2018; Kalinke et al., 2020). After chemical treatments (black circle) there was a reduction in the diameter of the Nyquist semicircle providing the Rct value of 867 Ω. The electron transfer for the treated electrode (rGO-PLA) was facilitated since there was a reduction of about 2-fold in the Rct value. These results corroborated with those achieved by SEM, Raman, and cyclic voltammetry, in which better electrochemical performances were acquired after the electrode surface treatment process that exposed the electroactive graphene sites and generated rGO.

Using the Kochi method (Bard et al., 2001; Klingler and Kochi, 1981) the heterogeneous electron transfer (HET) rate constant (k^0) of the rGO-PLA surface was calculated via cyclic voltammetry at different scan rates employing 1.0 mmol L^{-1} FcMeOH as redox probe and 0.1 mol L^{-1} KCl solution at different scan rates (50 to 250 mV s^{-1}) as shown in ~~(~~Figure S4~~)~~. The obtained value was estimated as 0.00235 cm s^{-1}. This result is about 3-fold higher than that estimated for the G-PLA in previous

work in the literature (0.00083 cm s^{-1}) (Katic et al., 2019), indicating that the rGO-PLA surface provides a fast HET kinetics for the occurrence of electrochemical reactions, corroborating with the others characterization data and explaining the results displayed in Figure 2.

3.2. Voltammetric sensing of serotonin

After confirming the formation of rGO in the 3D-printed G-PLA electrodes treated with DMF/HNO_3/$NaBH_4$ (rGO-PLA) the applicability of the obtained electrodes will be presented next. For convenience, the novel electrode will be named as 3D-printed rGO-PLA.

The sensing of serotonin upon the chemically treated 3D-printed G-PLA was carried out as a proof-of-concept in synthetic urine samples. First, the electrochemical behavior of serotonin at the developed sensor was explored by cyclic voltammetry (Figure S5) in the presence of 10 μmol L^{-1} of the analyte utilizing a 0.2 mol L^{-1} phosphate buffer solution (pH 7.0) as background electrolyte. This buffer is the most widely employed in the literature as supporting electrolyte for the detection of serotonin using graphene (Adumitrăchioaie et al., 2019; Cernat et al., 2020; Han et al., 2013; Kim et al., 2012). It is possible to note the appearance of an anodic peak around +0.25 V (*vs* G-PLA), being possible to conclude, from these results, that the proposed sensor has a great potential for the determination of serotonin since a very-well defined peak was acquired.

Next, to obtain a better electroanalytical performance towards serotonin sensing, the proposed method was carefully optimized regarding the most sensitive electrochemistry technique (square wave voltammetry (SWV) or differential pulse

voltammetry (DPV)) and the respective parameters (operational conditions) that influence the selected voltammetry technique, as well as the pH of the background electrolyte. These techniques were chosen based on works published in the literature (De Irazu et al., 2001; Fayemi et al., 2017; Jin et al., 2004; Mazloum-Ardakani and Khoshroo, 2014; Ramos et al., 2020; Satyanarayana et al., 2014; Yadav et al., 2020). For this, a study in the presence of 10 μmol L^{-1} serotonin was conducted via SWV and then DPV (Figure S6). DPV and SWV parameters were selected considering the maintenance of the same scan rate (30 mV s^{-1}) using both techniques. Figure S6 shows that the DPV technique provided a better voltammetric profile in addition to a greater current signal, in which the peak current increased by approximately 60% when compared to the SWV technique. Therefore, the DPV technique was selected for future procedures.

The effects of the scan rate, modulation amplitude and modulation time on the serotonin analytical signal were diligently explored in the intervals between 10 and 30 mV s^{-1}, 10 and 100 mV, and 0.01 and 0.1 s, respectively, as shown in Figure S7. When using 15 mV s^{-1}, 100 mV, and 0.01 s as scan rate, modulation amplitude, and modulation time, respectively, very-well defined peaks, lower deviation and higher peak currents were acquired. Therefore, these DPV parameters were used for further studies involving serotonin. Finally, the pH of the background electrolyte (0.2 mol L^{-1} of phosphate buffer) was evaluated in the range between 6.0 and 8.0, it is possible to achieve better analytical results when pH 7.0 was used. In this way, this value was employed in subsequent studies.

Under optimized conditions, the obtained voltammograms for increasing concentrations of serotonin are shown in Figure 5A. T~~t~~he plot of peak current against serotonin concentration exhibited a linear behavior in the range of ~~0.1~~ 0.3 μmol L^{-1} to

10 µmol L^{-1} with a satisfactory determination coefficient (R^2) of 0.997 (Figure ~~6A~~5B). The relation between peak current (I_p, A) and serotonin concentration ($C_{serotonin}$, µmol L^{-1}) can be described by the equation Ip = 4.6816 × 10^{-8} ± 3.71695 × 10^{-8} + 0.3041 ± 0.00724 $C_{serotonin}$. The relative standard deviation (RSD) value (calculated according to Skoog et. al. (2015) following: RSD = (s/$\bar{x}$) *100%, where s is the standard deviation and $\bar{x}$ the average of standard deviation values (Skoog et al., 2015)) was estimated as ~~2.2~~ 1.4% for four consecutive measurements using a low concentration of serotonin (~~10.0~~ 1.0 µmol L^{-1}). The LOD was estimated as 0.032 µmol L^{-1} following the IUPAC recommendations (by using the signal-to-noise method) following: LOD = 3xSD_{blank}/S, in which SD_{blank} is the standard deviation of baseline noise (n = 10) and S is the slope of the analytical curve. The inter-device precision (% RSD) was calculated as ~~3.3~~ 2.7% (n = 4, ~~10.0~~ 1.0 µmol L^{-1} level), as shown in Figure S8. According to some previous works (Katseli et al., 2020, 2019; López Marzo et al., 2020; Richter et al., 2019), when the RSD value is lower than 10% between devices, the reproducibility of the sensor is considered as adequate, in this sense we concluded that the proposed sensors provided acceptable manufacturing reproducibility. The stability of the sensor was assessed by consecutive measurements during five different days (n=5). Using a solution containing 1.0 µmol L^{-1} serotonin, a decrease of about 4.3% at the analytical signal (peak current) was observed between the first day of measurement and the last, showing that the manufactured sensor provided adequate stability. After this period (5 days), a large decline in the analytical signal and inaccurate measurements were observed.

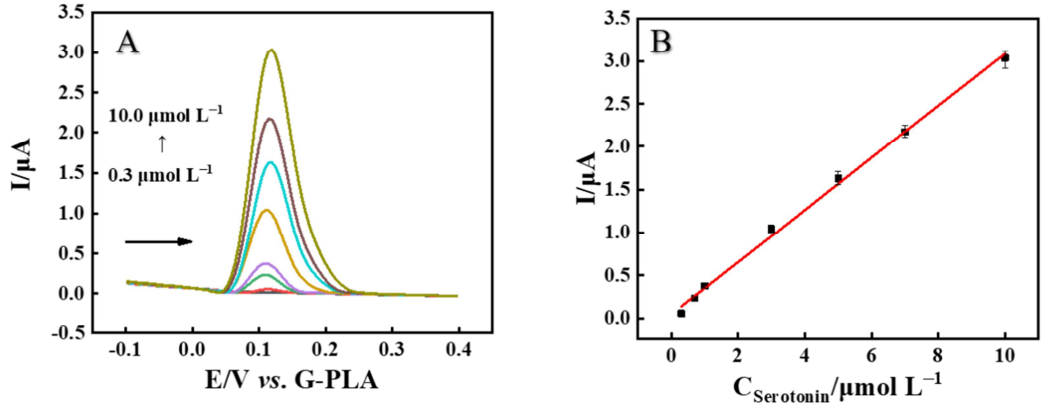

Figure 5. (A) DPV recordings for increasing serotonin concentrations (0.3, 0.7, 1.0, 3.0, 5.0, 7.0 and 10.0 µ mol L^{-1}) obtained on the rGO-PLA electrode (n = 3); black line correspond to the blank solution. **(B)** Respective analytical curve. DPV experimental conditions: modulation amplitude: 100 mV; modulation time: 0.01 s; scan rate: 15 mV s^{-1}. Background electrolyte: 0.2 mol L^{-1} phosphate buffer (pH 7.0).

The proposed 3D-printed rGO-PLA electrode was employed for serotonin determination (proof-of-concept) in synthetic urine samples. The samples were fortified with known amounts of the analyte and 15-fold diluted on the background electrolyte prior measurements. The results are summarized in Table S2. From the obtained results, it is possible to conclude that the developed sensor provided satisfactory analytical performance for serotonin sensing since acceptable recovery values (ranging from 95 to 111%) were acquired. This range of recovery values is accepted according to the literature and similar results can be found in previous works (Babaei and Babazadeh, 2011; Fayemi et al., 2017; Orzari et al., 2019; Ramos et al., 2020).

A selectivity study, in the serotonin sensing, was conducted by evaluating the interference caused by other species on the DPV signal of 1.0 µmol L^{-1} serotonin. The selected compounds as interfering species were: potassium chloride, sodium chloride,

creatinine, ammonium chloride, urea, sodium sulfate, and sodium dihydrogen phosphate, at two different ratios (1:10 and 1:100 (serotonin:interferent)), and for epinephrine, dopamine, and ascorbic and uric acids. In addition, besides two ratios already mentioned, the 1:1 ratio was also evaluated. These compounds were chosen based in some works published in the literature (Fayemi et al., 2017; Han et al., 2013; Kim et al., 2012; Mazloum-Ardakani and Khoshroo, 2014; Satyanarayana et al., 2014; Sharma et al., 2018). The results are provided in Table S3. Positive values are attributed to the increase in the serotonin voltammetric signal, while negative values are related to decrease in the serotonin signal due the presence of interfering species. As can be seen from the table, negligible or no interference was observed in the DPV signal of 1.0 µmol L^{-1} serotonin by the compounds: potassium, sodium and ammonium chlorides, sodium sulfate, sodium dihydrogen phosphate, creatinine, urea, and ascorbic acid, in all ratios. Although several works in the literature highlight that ascorbic acid interferes on the determination of serotonin (Fayemi et al., 2017; Han et al., 2013; Kim et al., 2012; Mazloum-Ardakani and Khoshroo, 2014; Satyanarayana et al., 2014; Sharma et al., 2018), the developed protocol was able to overcome this interference, as shown in Table S3, even at a concentration 100-fold higher. For epinephrine and dopamine, in the lowest ratio (1:1) there was also observed no interference; on the other hand, in ratios above 1:1, both molecules provided interference in the serotonin analytical signal. Additionally, it is possible to note in Table S3 that uric acid interferes in the detection of serotonin (even in the smallest ratio (1:1)). In this sense, a way to solve these interference problems caused by these compounds, would be the use modifiers for the working electrode surface with different active species, being possible to use composites, as shown in (Fayemi et al., 2017; Sharma et al., 2018). Therefore, these strategies will be considered in future works.

The proposed sensor provided satisfactory analytical performance (Table S~~3~~4) for the determination of serotonin, showing a linear range and LOD even better than other electrodes for determining this analyte described in the literature (Han et al., 2013; Jin et al., 2004; Mazloum-Ardakani and Khoshroo, 2014; Ramos et al., 2020; Satyanarayana et al., 2014). Even when different graphene nanomaterials were tested as modifiers for a glassy carbon electrode for serotonin detection (Kim et al., 2012), the obtained results were comparable to the one obtained in this work using a simple and disposable 3D-printed electrode containing the same material.

3.3. Voltammetric biosensing of catechol

Phenols and their derivatives (including catechol) appear in natural waters through industrial effluent discharges. Rubber processing industries, glues, adhesives, impregnating resins, electrical components (plastics), steel companies, among others, are responsible for the presence of phenols in natural waters. A limit of 0.5 mg L^{-1} is stipulated by the legislation of the State of São Paulo ("Decreto N^{o} 8.468," n.d.) and by the Federal Legislation ("Resolução CONAMA N^{o} 430 DE 13/05/2011 - Federal - LegisWeb," n.d.).

A catechol biosensor was fabricated using the 3D-printed rGO-PLA working electrode as a substrate modified with a enzyme layer composed by DHP and tyrosinase (Tyr-DHP/rGO-PLA) to quantify this substance in natural waters. For this, ~~T~~the electrochemical behavior of catechol onto the biosensor was first investigated by cyclic voltammetry (Figure ~~S7~~S9). It is possible to see that the response of the analyte was slightly better regarding the peak definition and peak current increase when compared to the working electrode in the absence of the Tyr-DHP film. It is noteworthy to mention

that the great advantage of using a biosensor is the gain of selectivity in determining catechol, that is, its ability to discriminate the analyte in the presence of different (concomitant) species, a function mainly attributed to immobilized biological material (Chang et al., 2002; Wang et al., 2008; Wee et al., 2019).

Tyr has been widely used in the construction of biosensors for the determination of phenols. This enzyme catalyzes oxidation reactions such as *o*-hydroxylation of monophenols to *o*-dihydroxy phenols and, subsequently, oxidation of *o*-dihydroxy phenols to *o*-quinones, all in the presence of molecular oxygen (Apetrei et al., 2011; Janegitz et al., 2012; Rescigno et al., 2002; Védrine et al., 2003; Vidal et al., 2008). The *o*-quinones can be reduced electrochemically without any mediator using a low potential. Thus, phenolic compounds (including catechol) can be selectively determined *via* electrochemical reduction of the *o*-quinones generated (Zhou et al., 2007; Zhou and Zhi, 2006), which was explored in this work.

The most sensitive voltammetric technique using the Tyr-DHP/rGO-PLA towards catechol biosensing was checked between SWV and DPV. The results are shown in Figure S10. As can be seen, the SWV technique provided a higher cathodic current signal around +0.05 V *vs* G-PLA/DMF. Utilizing the SWV, the cathodic peak current was about 2-fold higher than that obtained *via* the DPV technique. Therefore, the SWV was chosen for the next measurements.

The influence of SWV parameters: step potential, modulation amplitude, and frequency were evaluated in the range of −1 to −10 mV, 10 to 100 mV, and 10 to 100 Hz, respectively, as shown in Figure S11. The optimized parameter values were chosen taking into account better analytical responses, therefore, a step potential of −1 mV, modulation amplitude of 80 mV, and a frequency of 10 Hz were chosen for catechol determination.

Utilizing the conditions above-mentioned (optimized conditions), an analytical curve was obtained for increasing concentrations of catechol (Figure 6 A), and the proposed protocol, using the Tyr-DHP/rGO-PLA biosensor, provided wide linearity (R^2 = 0.999) in the range of 30 to 700 µmol L^{-1} (Figure 6B), corresponding to the equation Ip (A) = $-2.9571 \times 10^{-6} \pm 2.6271 \times 10^{-7} + 0.29808 \pm 0.00755$ $C_{catechol}$ (µmol L^{-1}). The intra-electrode precision (% RSD) was calculated as 1.5% for four consecutive measurements using a low concentration of catechol (100 µmol L^{-1}). The LOD was estimated as 0.26 µmol L^{-1}, following the same way of calculation used for serotonin. The inter-device precision (% RSD) was calculated as 8.0% (n = 4, 100 µmol L^{-1} level), indicating adequate manufacturing reproducibility. Similar results of reproducibility study were found in previous works (Erkmen et al., 2020; Laranjo et al., 2019). The stability of the proposed biosensor was evaluated in the same way for the sensor (n=5; five different days). Employing a solution containing 100 µmol L^{-1} catechol, a decrease of about 5.3% in the analytical signal (peak current) was acquired, showing that the fabricated biosensor provided adequate stability. After 5 days a great loss in the stability of the sensor and biosensor was observed, leading to inaccurate measurements with great loss in the performance.

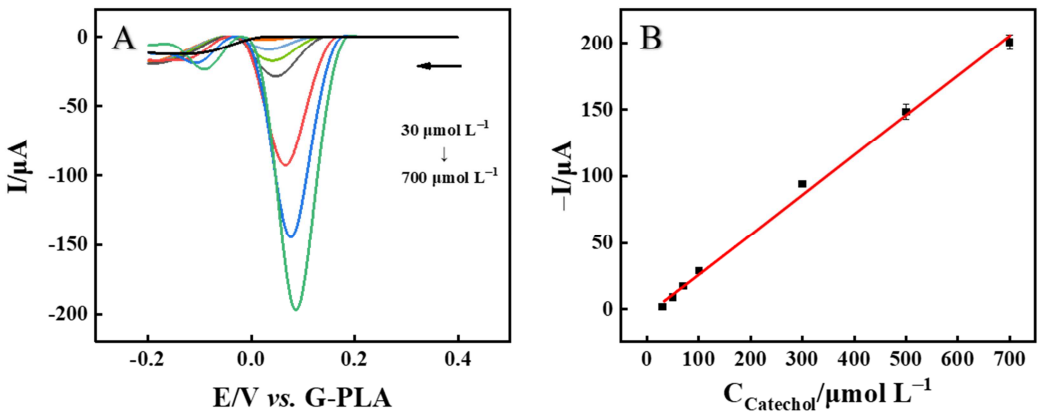

Figure 6. (A) SWV recordings for increasing catechol concentrations (30, 50, 70, 100, 300, 500 and 700 μmol L^{-1}). **(B)** Respective analytical curve for measurements in triplicate. SWV experimental conditions: step potential: −1 mV; modulation amplitude: 80 mV; frequency: 10 Hz. Background electrolyte: 0.2 mol L^{-1} phosphate buffer (pH 6.0).

The proposed Tyr-DHP/rGO-PLA biosensor was applied for biosensing of catechol (proof-of-concept) in water samples. The samples were fortified with known amounts of the analyte and subsequently diluted on the background electrolyte before analysis. The acquired results are shown in Table S45. From the table, it is possible to conclude that the developed protocol, using the proposed biosensor provided satisfactory analytical performance for catechol biosensing since adequate recovery results (in the range of 91 to 104%) were achieved.

A selectivity study was also accomplished for catechol sensing, in order to evaluate the interference caused by other species in the SWV signal of 70 μmol L^{-1} catechol. The study was performed by recording SWVs for catechol in presence of calcium chloride dihydrate, potassium chloride, sodium nitrate, sodium sulfate, lead (II) nitrate, dopamine, and hydroquinone at the ratios of 1:10 and 1:100 (catechol:interferent). The signal variation values obtained for catechol are presented in Table S6. No significative interference of calcium chloride dihydrate, potassium chloride, and sodium sulfate was observed when these compounds were 10 or 100 times more concentrated then catechol (Table S6). Lead (II) nitrate was considered as an interferent only when present in high concentrations (1:100 in comparison with catechol). However, as lead is a toxic metal, the concentration found in natural waters should be lower (10 μg L^{-1} is the upper limit for this metal in natural waters according

to World Health Organization agency) ("WHO Guidelines for Drinking-water Quality," 2011), thus, lead (II) nitrate is not an interferent for catechol determination. Sodium nitrate only affects the catechol signal when in high proportions (1:100). As a limitation of this sensor, the presence of dopamine and hydroquinone affected significantly the detection of catechol in waters in a way that the current response was strongly affected even in a 1:1 proportion with catechol, thus no signal variation was presented in the table. However, some strategies could be employed in the future as a way to circumvent this situation, such as the use of modifiers for composite electrodes (incorporation of other materials in the production of the film), which can enable the simultaneous determination of hydroquinone and catechol, as reported in the literature (Du et al., 2011; Guo et al., 2012; Song et al., 2015; Sunil Kumar Naik and Kumara Swamy, 2017; Zhang et al., 2015; Zheng et al., 2013). Thus, as future perspectives, the improvement in the selectivity of the proposed biosensor could be achieved.

The performance of Tyr-DHP/rGO-PLA biosensor was compared with other tyrosinase-based biosensors (Camargo et al., 2018; Erkmen et al., 2020; Kurbanoglu and Ozkan, 2018; Laranjo et al., 2019), with the analytical features indicated in Table S7. Tyr-DHP/rGO-PLA performed similarly to following biosensors in terms of linear range and LOD, but the device was advantageous concerning fast response, proper selectivity, and easy handling.

4. Conclusion

We have demonstrated a novel chemical treatment involving the sequential DMF/HNO_3/$NaBH_4$ reagents to generate rGO within 3D-printed PLA electrodes. The rGO-PLA electrodes presented a remarkable current increase for the redox probe

FcMeOH in comparison with the same surface treated by DMF immersion for 15 min, which has been considered in previous works using such electrodes. It is important to mention that DMF is a toxic organic solvent, which makes this protocol less environmentally-friendly. Despite its use to remove insulating material from the electrode surface is well known in the literature, our research group has been trying to develop new routes which do not employ toxic organic solvents and make the protocol environmentally-friendly, which follows the principles of green chemistry. Also, The use of modifiers in rGO-PLA electrodes is an important way to improve the selectivity in further works. EIS measurements showed that the rGO-PLA electrode presented the lowest resistance to electron transfer. The electrochemical results corroborated with Raman spectra and surface roughness obtained by AFM image. The proposed rGO-PLA electrode was successfully applied for serotonin determination in synthetic urine using DPV with notable sensing properties in comparison with previous works. Additionally, the rGO-PLA surface was used to fabricate a catechol biosensor, which was capable of determining the analyte in natural water samples with acceptable analytical features. These two examples show that the novel and simple chemical DMF/HNO_3/$NaBH_4$ treatment generates rGO with 3D-printed PLA electrodes with outstanding sensing properties for biosensing applications. Moreover, we present a new configuration of a compact all-3D-printed electrochemical device containing the three electrodes.

Acknowledgments

We gratefully acknowledge the Brazilian funding agencies: São Paulo Research Foundation (FAPESP, grant# 2013/22127-2, grant#2017/21097-3, grant# 2017/23960-0, grant# 2019/26953-0), Minas Gerais Research Foundation (FAPEMIG, grant # APQ-03141-18), National Council for Scientific and Technological Development (CNPq,

grants #427731/2018-6, 307271/2017-0, 303338/2019-9), INCTBio (CNPq grant#465389/2014-7) and Coordination for the Improvement of Higher Education Personnel (CAPES, grant #001) for the financial support. We also acknowledge the Laboratory of Structural Characterization/Department of Materials Engineering (LCE/DEMa) of the Federal University of São Carlos for SEM measurements and the Institute of Physics (INFIS) of the Federal University of Uberlandia for Raman (Horiba LabRAM HR Evolution Raman) spectroscopic measurements supported by the grant "Pró-Equipamentos" from the Brazilian agency CAPES and by FINEP.

5. References

Adams, A., Malkoc, A., La Belle, J.T., 2018. The Development of a Glucose Dehydrogenase 3D-Printed Glucose Sensor: A Proof-of-Concept Study. J. Diabetes Sci. Technol. 12, 176–182. doi:10.1177/1932296817715272

Adumitrăchioaie, A., Tertiș, M., Suciu, M., Graur, F., Cristea, C., 2019. A novel immunosensing platform for serotonin detection in complex real samples based on graphene oxide and chitosan. Electrochim. Acta 311, 50–61. doi:10.1016/j.electacta.2019.04.128

Apetrei, C., Rodríguez-Méndez, M.L., De Saja, J.A., 2011. Amperometric tyrosinase based biosensor using an electropolymerized phosphate-doped polypyrrole film as an immobilization support. Application for detection of phenolic compounds. Electrochim. Acta 56, 8919–8925. doi:10.1016/j.electacta.2011.07.127

Au, A.K., Huynh, W., Horowitz, L.F., Folch, A., 2016. 3D-Printed Microfluidics. Angew. Chemie Int. Ed. 55, 3862–3881. doi:10.1002/anie.201504382

Babaei, A., Babazadeh, M., 2011. A selective simultaneous determination of levodopa and serotonin using a glassy carbon electrode modified with multiwalled carbon nanotube/chitosan composite. Electroanalysis 23, 1726–1735. doi:10.1002/elan.201000755

Bard, A.J., Faulkner, L.R., 2001. Electrochemical Methods: Fundamentals and Applications, 2nd Edition. John Wiley & Sons, New York.

Browne, M.P., Novotný, F., Sofer, Z., Pumera, M., 2018. 3D Printed Graphene Electrodes' Electrochemical Activation. ACS Appl. Mater. Interfaces 10, 40294–40301. doi:10.1021/acsami.8b14701

Camargo, J.R., Baccarin, M., Raymundo-Pereira, P.A., Campos, A.M., Oliveira, G.G., Fatibello-Filho, O., Oliveira, O.N., Janegitz, B.C., 2018. Electrochemical biosensor made with tyrosinase immobilized in a matrix of nanodiamonds and potato starch for detecting phenolic compounds. Anal. Chim. Acta 1034, 137–143. doi:10.1016/j.aca.2018.06.001

Cardoso, R.M., Castro, S.V.F., Silva, M.N.T., Lima, A.P., Santana, M.H.P., Nossol, E., Silva, R.A.B., Richter, E.M., Paixão, T.R.L.C., Muñoz, R.A.A., 2019. 3D-printed flexible device combining sampling and detection of explosives. Sensors Actuators, B Chem. 292, 308–313. doi:10.1016/j.snb.2019.04.126

Cardoso, R.M., Kalinke, C., Rocha, R.G., dos Santos, P.L., Rocha, D.P., Oliveira, P.R., Janegitz, B.C., Bonacin, J.A., Richter, E.M., Munoz, R.A.A., 2020a. Additive-manufactured (3D-printed) electrochemical sensors: A critical review. Anal. Chim. Acta 1118, 73–91. doi:10.1016/j.aca.2020.03.028

Cardoso, R.M., Mendonça, D.M.H., Silva, W.P., Silva, M.N.T., Nossol, E., da Silva, R.A.B., Richter, E.M., Muñoz, R.A.A., 2018. 3D printing for electroanalysis: From multiuse electrochemical cells to sensors. Anal. Chim. Acta 1033, 49–57.

doi:10.1016/j.aca.2018.06.021

Cardoso, R.M., Silva, P.R.L., Lima, A.P., Rocha, D.P., Oliveira, T.C., do Prado, T.M., Fava, E.L., Fatibello-Filho, O., Richter, E.M., Muñoz, R.A.A., 2020b. 3D-Printed graphene/polylactic acid electrode for bioanalysis: Biosensing of glucose and simultaneous determination of uric acid and nitrite in biological fluids. Sensors Actuators B Chem. 307, 127621. doi:10.1016/j.snb.2019.127621

Cernat, A., Ştefan, G., Tertis, M., Cristea, C., Simon, I., 2020. An overview of the detection of serotonin and dopamine with graphene-based sensors. Bioelectrochemistry 136, 107620. doi:10.1016/j.bioelechem.2020.107620

Chang, S.C., Rawson, K., McNeil, C.J., 2002. Disposable tyrosinase-peroxidase bi-enzyme sensor for amperometric detection of phenols. Biosens. Bioelectron. 17, 1015–1023. doi:10.1016/S0956-5663(02)00094-5

Chen, W.Q., Veksha, A., Lisak, G., 2020. Graphene-like carbon nanosheets grown over alkali-earth metal oxides: Effects of chemical composition and physico-chemical properties. Carbon N. Y. 159, 378–389. doi:10.1016/j.carbon.2019.12.048

Cocovi-Solberg, D.J., Worsfold, P.J., Miró, M., 2018. Opportunities for 3D printed millifluidic platforms incorporating on-line sample handling and separation. TrAC - Trends Anal. Chem. 108, 13–22. doi:10.1016/j.trac.2018.08.007

de Araujo Andreotti, I.A., Orzari, L.O., Camargo, J.R., Faria, R.C., Marcolino-Junior, L.H., Bergamini, M.F., Gatti, A., Janegitz, B.C., 2019. Disposable and flexible electrochemical sensor made by recyclable material and low cost conductive ink. J. Electroanal. Chem. 840, 109–116. doi:10.1016/j.jelechem.2019.03.059

De Irazu, S., Unceta, N., Sampedro, M.C., Goicolea, M.A., Barrio, R.J., 2001. Multimembrane carbon fiber microelectrodes for amperometric determination of serotonin in human urine. Analyst 126, 495–500. doi:10.1039/b009703i

Decreto N° 8.468 [WWW Document], n.d. URL https://licenciamento.cetesb.sp.gov.br/legislacao/estadual/decretos/1976_Dec_Est_8468.pdf (accessed 5.21.20).

dos Santos, P.L., Katic, V., Loureiro, H.C., dos Santos, M.F., dos Santos, D.P., Formiga, A.L.B., Bonacin, J.A., 2019. Enhanced performance of 3D printed graphene electrodes after electrochemical pre-treatment: Role of exposed graphene sheets. Sensors Actuators, B Chem. 281, 837–848. doi:10.1016/j.snb.2018.11.013

Du, H., Ye, J., Zhang, J., Huang, X., Yu, C., 2011. A voltammetric sensor based on graphene-modified electrode for simultaneous determination of catechol and hydroquinone. J. Electroanal. Chem. 650, 209–213. doi:10.1016/J.JELECHEM.2010.10.002

Erkmen, C., Kurbanoglu, S., Uslu, B., 2020. Fabrication of poly(3,4-ethylenedioxythiophene)-iridium oxide nanocomposite based Tyrosinase biosensor for the dual detection of catechol and azinphos methyl. Sensors Actuators, B Chem. 316, 128121. doi:10.1016/j.snb.2020.128121

Fayemi, O.E., Adekunle, A.S., Ebenso, E.E., 2017. Electrochemical determination of serotonin in urine samples based on metal oxide nanoparticles/MWCNT on modified glassy carbon electrode. Sens. Bio-Sensing Res. 13, 17–27. doi:10.1016/j.sbsr.2017.01.005

Foster, C.W., Elbardisy, H.M., Down, M.P., Keefe, E.M., Smith, G.C., Banks, C.E., 2020. Additively manufactured graphitic electrochemical sensing platforms. Chem. Eng. J. 381, 122343. doi:10.1016/j.cej.2019.122343

Gulzar, U., Glynn, C., O'Dwyer, C., 2019. Additive manufacturing for energy storage: Methods, designs and materials selection for customizable 3D printed batteries and supercapacitors. Curr. Opin. Electrochem. 20, 46–53.

doi:10.1016/j.coelec.2020.02.009

Guo, Q., Huang, J., Chen, P., Liu, Y., Hou, H., You, T., 2012. Simultaneous determination of catechol and hydroquinone using electrospun carbon nanofibers modified electrode. Sensors Actuators, B Chem. 163, 179–185. doi:10.1016/j.snb.2012.01.032

Gusmão, R., Browne, M.P., Sofer, Z., Pumera, M., 2019. The capacitance and electron transfer of 3D-printed graphene electrodes are dramatically influenced by the type of solvent used for pre-treatment. Electrochem. commun. 102, 83–88. doi:10.1016/j.elecom.2019.04.004

Hamzah, H.H., Shafiee, S.A., Abdalla, A., Patel, B.A., 2018. 3D printable conductive materials for the fabrication of electrochemical sensors: A mini review. Electrochem. commun. 96, 27–31. doi:10.1016/j.elecom.2018.09.006

Han, H.S., You, J.M., Jeong, H., Jeon, S., 2013. Synthesis of graphene oxide grafted poly(lactic acid) with palladium nanoparticles and its application to serotonin sensing. Appl. Surf. Sci. 284, 438–445. doi:10.1016/j.apsusc.2013.07.116

Honeychurch, K.C., Rymansaib, Z., Iravani, P., 2018. Anodic stripping voltammetric determination of zinc at a 3-D printed carbon nanofiber–graphite–polystyrene electrode using a carbon pseudo-reference electrode. Sensors Actuators B Chem. 267, 476–482. doi:10.1016/j.snb.2018.04.054

Hughes, J.P., Dos Santos, L., Down, M.P., Foster, C.W., Bonacin, J.A., Keefe, E.M., Rowley-Neale, S.J., Banks, C.E., 2020. Single step additive manufacturing (3D printing) of electrocatalytic anodes and cathodes for efficient water splitting. Sustain. Energy Fuels 4, 302–311. doi:10.1039/c9se00679f

Janegitz, B.C., Dos Santos, F.A., Faria, R.C., Zucolotto, V., 2014. Electrochemical determination of estradiol using a thin film containing reduced graphene oxide and

dihexadecylphosphate. Mater. Sci. Eng. C 37, 14–19. doi:10.1016/j.msec.2013.12.026

Janegitz, B.C., Medeiros, R.A., Rocha-filho, R.C., Fatibello-filho, O., 2012. Diamond & Related Materials Direct electrochemistry of tyrosinase and biosensing for phenol based on gold nanoparticles electrodeposited on a boron-doped diamond electrode. Diam. Relat. Mater. 25, 128–133. doi:10.1016/j.diamond.2012.02.023

Jin, G.P., Lin, X.Q., Gong, J.M., 2004. Novel choline and acetylcholine modified glassy carbon electrodes for simultaneous determination of dopamine, serotonin and ascorbic acid. J. Electroanal. Chem. 569, 135–142. doi:10.1016/j.jelechem.2004.02.022

Kalinke, C., Neumsteir, N.V., Aparecido, G.D.O., Ferraz, T.V.D.B., Dos Santos, P.L., Janegitz, B.C., Bonacin, J.A., 2020. Comparison of activation processes for 3D printed PLA-graphene electrodes: Electrochemical properties and application for sensing of dopamine. Analyst 145, 1207–1218. doi:10.1039/c9an01926j

Katic, V., Dos Santos, P.L., Dos Santos, M.F., Pires, B.M., Loureiro, H.C., Lima, A.P., Queiroz, J.C.M., Landers, R., Muñoz, R.A.A., Bonacin, J.A., 2019. 3D Printed Graphene Electrodes Modified with Prussian Blue: Emerging Electrochemical Sensing Platform for Peroxide Detection. ACS Appl. Mater. Interfaces 11, 35068–35078. doi:10.1021/acsami.9b09305

Katseli, V., Economou, A., Kokkinos, C., 2020. A novel all-3D-printed cell-on-a-chip device as a useful electroanalytical tool: Application to the simultaneous voltammetric determination of caffeine and paracetamol. Talanta 208, 120388. doi:10.1016/j.talanta.2019.120388

Katseli, V., Economou, A., Kokkinos, C., 2019. Single-step fabrication of an integrated 3D-printed device for electrochemical sensing applications. Electrochem. commun.

103, 100–103. doi:10.1016/j.elecom.2019.05.008

Kim, S.K., Kim, D., Jeon, S., 2012. Electrochemical determination of serotonin on glassy carbon electrode modified with various graphene nanomaterials. Sensors Actuators, B Chem. 174, 285–291. doi:10.1016/j.snb.2012.08.034

Klingler, R.J., Kochi, J.K., 1981. Electron-transfer kinetics from cyclic voltammetry. Quantitative description of electrochemical reversibility. J. Phys. Chem. 85, 1731–1741. doi:10.1021/j150612a028

Kurbanoglu, S., Ozkan, S.A., 2018. A Novel Enzymatic Biosensor for the Detection of Catechol Using Multi-walled Carbon Nanotubes and Gold Nanowires. Electrocatalysis 9, 252–257. doi:10.1007/s12678-017-0408-4

Laranjo, M.T., Morawski, F.M., Dias, S.L.P., Benvenutti, E. V., Arenas, L.T., Costa, T.M.H., 2019. Silica/titania graphite composite modified with chitosan and tyrosinase employed as a sensitive biosensor for phenolic compounds. J. Braz. Chem. Soc. 30, 2660–2671. doi:10.21577/0103-5053.20190190

Laube, N., Mohr, B., Hesse, A., 2001. Laser-probe-based investigation of the evolution of particle size distributions of calcium oxalate particles formed in artificial urines. J. Cryst. Growth 233, 367–374. doi:10.1016/S0022-0248(01)01547-0

López Marzo, A.M., Mayorga-Martinez, C.C., Pumera, M., 2020. 3D-printed graphene direct electron transfer enzyme biosensors. Biosens. Bioelectron. 151, 111980. doi:10.1016/j.bios.2019.111980

Manzanares-Palenzuela, C.L., Hermanova, S., Sofer, Z., Pumera, M., 2019. Proteinase-sculptured 3D-printed graphene/polylactic acid electrodes as potential biosensing platforms: Towards enzymatic modeling of 3D-printed structures. Nanoscale 11, 12124–12131. doi:10.1039/c9nr02754h

Manzanares Palenzuela, C.L., Novotný, F., Krupička, P., Sofer, Z., Pumera, M., 2018.

3D-Printed Graphene/Polylactic Acid Electrodes Promise High Sensitivity in Electroanalysis. Anal. Chem. 90, 5753–5757. doi:10.1021/acs.analchem.8b00083

Mazloum-Ardakani, M., Khoshroo, A., 2014. High sensitive sensor based on functionalized carbon nanotube/ionic liquid nanocomposite for simultaneous determination of norepinephrine and serotonin. J. Electroanal. Chem. 717–718, 17–23. doi:10.1016/j.jelechem.2013.12.034

Ngo, T.D., Kashani, A., Imbalzano, G., Nguyen, K.T.Q., Hui, D., 2018. Additive manufacturing (3D printing): A review of materials, methods, applications and challenges. Compos. Part B Eng. 143, 172–196. doi:10.1016/j.compositesb.2018.02.012

Nielsen, A. V., Beauchamp, M.J., Nordin, G.P., Woolley, A.T., 2020. 3D Printed Microfluidics. Annu. Rev. Anal. Chem. 13. doi:10.1146/annurev-anchem-091619-102649

Novotný, F., Urbanová, V., Plutnar, J., Pumera, M., 2019. Preserving Fine Structure Details and Dramatically Enhancing Electron Transfer Rates in Graphene 3D-Printed Electrodes via Thermal Annealing: Toward Nitroaromatic Explosives Sensing. ACS Appl. Mater. Interfaces 11, 35371–35375. doi:10.1021/acsami.9b06683

O'Neil, G.D., 2020. Toward single-step production of functional electrochemical devices using 3D printing: Progress, challenges, and opportunities. Curr. Opin. Electrochem. 20, 60–65. doi:10.1016/j.coelec.2020.02.023

Orzari, L.O., Cristina de Freitas, R., Aparecida de Araujo Andreotti, I., Gatti, A., Janegitz, B.C., 2019. A novel disposable self-adhesive inked paper device for electrochemical sensing of dopamine and serotonin neurotransmitters and biosensing of glucose. Biosens. Bioelectron. 138, 111310.

doi:10.1016/j.bios.2019.05.015

Pang, Y., Cao, Y., Chu, Y., Liu, M., Snyder, K., MacKenzie, D., Cao, C., 2020. Additive Manufacturing of Batteries. Adv. Funct. Mater. 30, 1906244. doi:10.1002/adfm.201906244

Ramos, M.M.V., Carvalho, J.H.S., de Oliveira, P.R., Janegitz, B.C., 2020. Determination of serotonin by using a thin film containing graphite, nanodiamonds and gold nanoparticles anchored in casein. Meas. J. Int. Meas. Confed. 149, 106979. doi:10.1016/j.measurement.2019.106979

Rescigno, A., Sollai, F., Pisu, B., Rinaldi, A., Sanjust, E., 2002. Tyrosinase inhibition: General and applied aspects. J. Enzyme Inhib. Med. Chem. 17, 207–218. doi:10.1080/14756360210000010923

Resolução CONAMA Nº 430 DE 13/05/2011 - Federal - LegisWeb [WWW Document], n.d. URL https://www.legisweb.com.br/legislacao/?id=114770 (accessed 5.21.20).

Richter, E.M., Rocha, D.P., Cardoso, R.M., Keefe, E.M., Foster, C.W., Munoz, R.A.A., Banks, C.E., 2019. Complete Additively Manufactured (3D-Printed) Electrochemical Sensing Platform. Anal. Chem. 91, 12844–12851. doi:10.1021/acs.analchem.9b02573

Rocha, D.P., Dornellas, R.M., Cardoso, R.M., Narciso, L.C.D., Silva, M.N.T., Nossol, E., Richter, E.M., Munoz, R.A.A., 2018a. Chemically versus electrochemically reduced graphene oxide: Improved amperometric and voltammetric sensors of phenolic compounds on higher roughness surfaces. Sensors Actuators, B Chem. 254, 701–708. doi:10.1016/j.snb.2017.07.070

Rocha, D.P., Foster, C., Keefe, E., Munoz, R.A.A., Buller, G., Banks, C.E., 2020. Trace manganese detection via differential pulse cathodic stripping voltammetry using

disposable electrodes: additively manufactured nanographite electrochemical sensing platforms. Analyst 145, 3424–3430. doi:10.1039/d0an00018c

Rocha, D.P., Silva, M.N.T., Cardoso, R.M., Castro, S.V.F., Tormin, T.F., Richter, E.M., Nossol, E., Munoz, R.A.A., 2018b. Carbon nanotube/reduced graphene oxide thin-film nanocomposite formed at liquid-liquid interface: Characterization and potential electroanalytical applications. Sensors Actuators, B Chem. 269, 293–303. doi:10.1016/j.snb.2018.04.147

Rocha, D.P., Squissato, A.L., da Silva, S.M., Richter, E.M., Munoz, R.A.A., 2020. Improved electrochemical detection of metals in biological samples using 3D-printed electrode: Chemical/electrochemical treatment exposes carbon-black conductive sites. Electrochim. Acta 335, 135688. doi:10.1016/j.electacta.2020.135688

Satyanarayana, M., Koteshwara Reddy, K., Vengatajalabathy Gobi, K., 2014. Nanobiocomposite Based Electrochemical Sensor for Sensitive Determination of Serotonin in Presence of Dopamine, Ascorbic Acid and Uric Acid In Vitro. Electroanalysis 26, 2365–2372. doi:10.1002/elan.201400243

Sharma, S., Singh, N., Tomar, V., Chandra, R., 2018. A review on electrochemical detection of serotonin based on surface modified electrodes. Biosens. Bioelectron. 107, 76–93. doi:10.1016/j.bios.2018.02.013

Skoog, D.A., West, D.M., Holler, F.J., Couch, S.R., 2015. Fundamentals of analytical chemistry, eighth. ed. Thomson, São Paulo. doi:10.1016/S0584-8547

Song, D., Xia, J., Zhang, F., Bi, S., Xiang, W., Wang, Z., Xia, L., Xia, Y., Li, Y., Xia, L., 2015. Multiwall carbon nanotubes-poly(diallyldimethylammonium chloride)-graphene hybrid composite film for simultaneous determination of catechol and hydroquinone. Sensors Actuators, B Chem. 206, 111–118.

doi:10.1016/j.snb.2014.08.084

Sunil Kumar Naik, T.S., Kumara Swamy, B.E., 2017. Modification of carbon paste electrode by electrochemical polymerization of neutral red and its catalytic capability towards the simultaneous determination of catechol and hydroquinone: A voltammetric study. J. Electroanal. Chem. 804, 78–86. doi:10.1016/j.jelechem.2017.08.047

Védrine, C., Fabiano, S., Tran-Minh, C., 2003. Amperometric tyrosinase based biosensor using an electrogenerated polythiophene film as an entrapment support. Talanta 59, 535–544. doi:10.1016/S0039-9140(02)00540-4

Vidal, J.C., Bonel, L., Castillo, J.R., 2008. A modulated tyrosinase enzyme-based biosensor for application to the detection of dichlorvos and atrazine pesticides. Electroanalysis 20, 865–873. doi:10.1002/elan.200704115

Wang, S., Tan, Y., Zhao, D., Liu, G., 2008. Amperometric tyrosinase biosensor based on Fe3O4 nanoparticles-chitosan nanocomposite. Biosens. Bioelectron. 23, 1781–1787. doi:10.1016/j.bios.2008.02.014

Wee, Y., Park, S., Kwon, Y.H., Ju, Y., Yeon, K.M., Kim, J., 2019. Tyrosinase-immobilized CNT based biosensor for highly-sensitive detection of phenolic compounds. Biosens. Bioelectron. 132, 279–285. doi:10.1016/j.bios.2019.03.008

WHO Guidelines for Drinking-water Quality [WWW Document], 2011. URL https://www.who.int/water_sanitation_health/publications/2011/dwq_guidelines/en/ (accessed 8.21.20)

Wirth, D.M., Sheaff, M.J., Waldman, J. V., Symcox, M.P., Whitehead, H.D., Sharp, J.D., Doerfler, J.R., Lamar, A.A., Leblanc, G., 2019. Electrolysis Activation of Fused-Filament-Fabrication 3D-Printed Electrodes for Electrochemical and Spectroelectrochemical Analysis. Anal. Chem. 91, 5553–5557.

doi:10.1021/acs.analchem.9b01331

Yadav, V., Raj, M., Goyal, R.N., 2020. Comparison of Different Unmodified and Nano-Material Modified Sensors for the Ultrasensitive Determination of Serotonin. J. Electrochem. Soc. 167, 27539. doi:10.1149/1945-7111/ab6dd3

Yang, C., Cao, Q., Puthongkham, P., Lee, S.T., Ganesana, M., Lavrik, N. V., Venton, B.J., 2018. 3D-Printed Carbon Electrodes for Neurotransmitter Detection. Angew. Chemie Int. Ed. 57, 14255–14259. doi:10.1002/anie.201809992

Zhang, H., Huang, Y., Hu, S., Huang, Q., Wei, C., Zhang, W., Yang, W., Dong, P., Hao, A., 2015. Self-assembly of graphitic carbon nitride nanosheets-carbon nanotube composite for electrochemical simultaneous determination of catechol and hydroquinone. Electrochim. Acta 176, 28–35. doi:10.1016/j.electacta.2015.06.119

Zheng, L., Xiong, L., Li, Y., Xu, J., Kang, X., Zou, Z., Yang, S., Xia, J., 2013. Facile preparation of polydopamine-reduced graphene oxide nanocomposite and its electrochemical application in simultaneous determination of hydroquinone and catechol. Sensors Actuators, B Chem. 177, 344–349. doi:10.1016/j.snb.2012.11.006

Zhou, Y.L., Tian, R.H., Zhi, J.F., 2007. Amperometric biosensor based on tyrosinase immobilized on a boron-doped diamond electrode. Biosens. Bioelectron. 22, 822–828. doi:10.1016/j.bios.2006.03.001

Zhou, Y.L., Zhi, J.F., 2006. Development of an amperometric biosensor based on covalent immobilization of tyrosinase on a boron-doped diamond electrode. Electrochem. commun. 8, 1811–1816. doi:10.1016/j.elecom.2006.08.022

-A new platform using reduced graphene oxide is proposed

- The electrochemical cell, sensors, and biosensors were produced by 3D-printing

-The proposed electrode could be applied for other electrochemical sensing and biosensing

- The 3D-printed sensor and biosensor were applied for the determination of phenolic compounds

Declaration of interests

☒ The authors declare that they have no known competing financial interests or personal relationships that could have appeared to influence the work reported in this paper.

☐The authors declare the following financial interests/personal relationships which may be considered as potential competing interests: